Contents lists available at ScienceDirect

Polymer

journal homepage: www.elsevier.com/locate/polymer

Autonomic healing of PMMA via microencapsulated solvent

Asha-Dee N. Celestine [a, c], Nancy R. Sottos [b, c], Scott R. White [a, c, *]

[a] Department of Aerospace Engineering, University of Illinois at Urbana-Champaign, Urbana, IL 61801, USA
[b] Department of Materials Science and Engineering, University of Illinois at Urbana-Champaign, Urbana, IL 61801, USA
[c] Beckman Institute for Advanced Science and Technology, University of Illinois at Urbana-Champaign, Urbana, IL 61801, USA

ARTICLE INFO

ABSTRACT

Fully autonomous, room temperature self-healing in PMMA is achieved for the first time through the use of microcapsules containing a solvent. Linear PMMA is embedded with microcapsules (ca. 300 μm) containing a liquid anisole solvent core and a small amount of linear PMMA polymer for healing of crack damage. Specimens containing a range of concentrations of microcapsules were fracture tested and then allowed to heal for 1–7 days at ambient conditions. The healing efficiency of the material is evaluated based on the recovery of fracture toughness and is shown to be dependent on both healing time and microcapsule concentration. A maximum healing efficiency of 89% is obtained for specimens containing 5 wt% solvent microcapsules after 3 days of healing.

1. Introduction

Blood clotting, cell proliferation, the formation of scar tissue and other healing mechanisms in both plants and animals provide inspiration for the healing of damage in synthetic materials such as plastics, adhesives and polymer composites [1–16]. The first demonstration of fully autonomous self-healing in a polymeric material was achieved by embedding catalyst particles and monomer-filled microcapsules into an epoxy polymer system [1]. Material damage via propagating cracks ruptured the microcapsules and released the liquid monomer into the crack plane. The monomer then reacted with the catalyst particles to form new polymeric material in the crack plane thereby healing the damage and restoring mechanical properties to the polymer system.
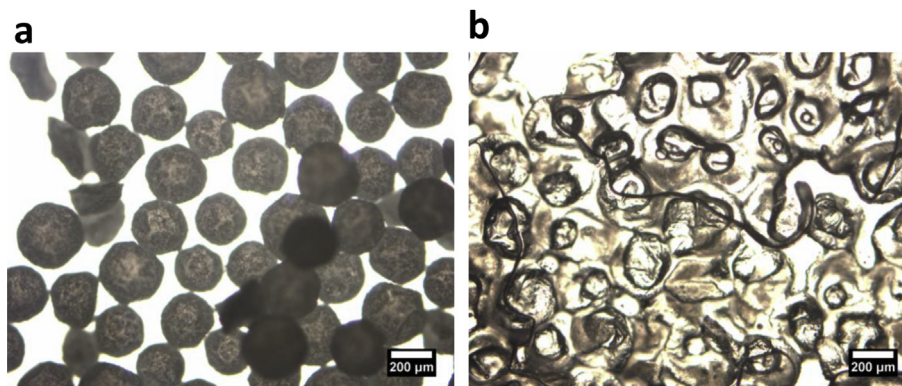
Since this first demonstration of self-healing, a number of different capsule based approaches have emerged relying on diverse strategies for sequestering the healing agent [17]. In addition to the capsule-catalyst system pioneered by White et al. [1] and utilized by other researchers [4,18], multi-capsule systems, where both the healing and polymerizing agent are encapsulated, have been used successfully [2,19,20]. Yet another scheme employs a phase separation technique whereby one of the healing components is phase separated in the polymer while the other component may be encapsulated [20,21]. Single capsule systems have also been used in which the healing agent is encapsulated and the polymerizing agent is some residual functionality in the polymer or an environmental stimulus [22–24]. One example of the use of a single capsule system is the solvent-based healing of epoxy demonstrated by Caruso et al. [22,23]. In their work, the mechanism for healing involves swelling of the epoxy matrix by the released solvent which then promotes additional cross-linking with residual amines in the partially cured matrix [23]. For thermoplastic repair the release of a good solvent (with respect to the thermoplastic matrix) into the damage zone can promote intrinsic crack healing [25].

Intrinsic crack healing in thermoplastics is mainly due to reptation of molecular chains and can be initiated via thermal, adhesive, or solvent mechanisms [26,27]. Traditionally, the repair of damage in thermoplastics such as poly(methyl methacrylate) (PMMA) has been achieved using thermal methods [26]. After damage, the material is heated to a temperature above its glass transition temperature (T_g) in order to mobilize polymer chains and initiate crack healing. Efforts to achieve healing in thermoplastics at ambient temperatures have included the immersion of entire specimens in appropriate solvents [28–30] and the incorporation of microcapsules filled with dichlorobenzene into the matrix material [31]. Both of these approaches, however, were non-autonomous and measures of healing were either significantly low or not provided altogether. What is required for autonomous self-healing thermoplastics is the encapsulation and uniform distribution of a good solvent that promotes excellent rebonding of the matrix crack surfaces.

* Corresponding author. Department of Aerospace Engineering, University of Illinois at Urbana-Champaign, 104 South Wright Street, Urbana, IL 61801, USA. Tel.: +1 217 333 1077.
E-mail address: swhite@illinois.edu (S.R. White).

Fig. 1. Optical images of poly(urethane)/urea-formaldehyde (PU/UF) microcapsules containing anisole solvent with dissolved PMMA. (a) Intact microcapsules. (b) Crushed microcapsules with released core.

Screening tests performed by Caruso have revealed a number of good solvents for PMMA [32]. A good solvent is one for which the interactions between the polymer segments and solvent molecules are more energetically favorable than those between the polymer segments themselves and is usually identified as one whose solubility parameter (δ) is close to that of the polymer [29,33]. Good solvents for PMMA include ethyl phenylacetate (EPA), phenylacetate (PA), chlorobenzene (PhCl) and anisole. Gladman et al. have recently demonstrated autonomous solvent healing in a bone cement thermoplastic system containing microcapsules with a liquid PMMA-anisole core material [33]. PMMA was added to the core solvent (anisole) to promote increased healing efficiency in small scale cracks within the bone cement system and to promote environmental stability of the microcapsules [33].

The efficiency of a solvent microcapsule system for autonomous healing in a thermoplastic polymer was investigated in this work. PMMA specimens containing PMMA-anisole microcapsules were prepared and subjected to Mode I fracture. The effects of healing time and microcapsule concentration on the recovery of fracture toughness were examined to determine the optimum conditions necessary for healing.

2. Materials and methods

2.1. Microcapsule synthesis

Double shell wall poly(urethane)/urea-formaldehyde (PU/UF) microcapsules filled with a core solution of 10 wt% PMMA (average $M_w \approx 350$ kDa; Sigma−Aldrich) dissolved in the solvent anisole (Sigma−Aldrich) were prepared using a single batch process adapted from Caruso et al. [6]. All materials were used as received. The solvent anisole was chosen as the healing agent because its solubility parameter is closest to that of PMMA. The PU prepolymer (4 g) was first dissolved in 60 mL of the core solution (10 wt% PMMA, 90 wt% anisole) and then added to the mixing vessel, which contained double the amount of UF reaction components prescribed by Caruso [6]. A stir rate of 500 revolutions per minute (rpm) was maintained throughout the reaction. The resulting microcapsules were then dried and sieved. Control microcapsules containing dicyclopentadiene (DCPD) monomer were produced using an identical protocol.

Microcapsules of diameter 250−355 μm were isolated and used in all experiments. Optical images of the microcapsules were acquired with a Leica DMR optical microscope and representative samples of the PU/UF microcapsules containing PMMA-anisole are shown in Fig. 1. Intact microcapsules are shown in Fig. 1a. The

microcapsules are fairly round in shape and possess a rough surface. In Fig. 1b, the microcapsules have been crushed and the released liquid core is visible.

2.2. PMMA synthesis

Linear PMMA was synthesized via free radical polymerization by reacting the monomer, methyl methacrylate (MMA) with an initiator, benzoyl peroxide (BPO) and an activator, N,N-dimethylaniline (DMA). MMA (Sigma−Aldrich) was first purified by running it through a column of basic alumina and then deoxygenated by sparging with argon for 30 min. BPO (Sigma−Aldrich) was purified by first dissolving it in acetone, followed by precipitation from two volumes of distilled water and then drying under vacuum at room temperature overnight. DMA (Sigma−Aldrich) was used as received. MMA and BPO were combined in a 25 mL scintillation vial. The vial was sealed and purged with argon for 30 s and then the solution was sparged with argon for 30 s. DMA was then added to the solution and the vial was purged and sparged again for 1 min. The exact amounts used during the PMMA synthesis are shown in Table 1.

2.3. Specimen geometry

Double cleavage drilled compression (DCDC) specimens were prepared under ambient conditions using a cell casting technique (Section 2.4). The DCDC test specimen is a column of rectangular cross-section with a central circular hole as shown in Fig. 2. The specimen is subjected to axial compression from which transverse tensile stresses are produced at the top and bottom crowns of the central hole. When the energy release rate is equal to the fracture toughness of the material, a stable Mode I crack is generated at each crown [34−38]. These cracks propagate along the mid-plane of the

Table 1
Recipe for linear PMMA containing solvent microcapsules. Amounts shown are per specimen.

	Amount used
Chemical species	
Methyl methacrylate (MMA)	4.0 mL
Benzoyl peroxide (BPO)	0.06 g
N,N-dimethylaniline (DMA)	24.0 μL
Microcapsule concentration (wt%)	
2.5	0.106 g
5.0	0.211 g
7.5	0.317 g
10.0	0.422 g

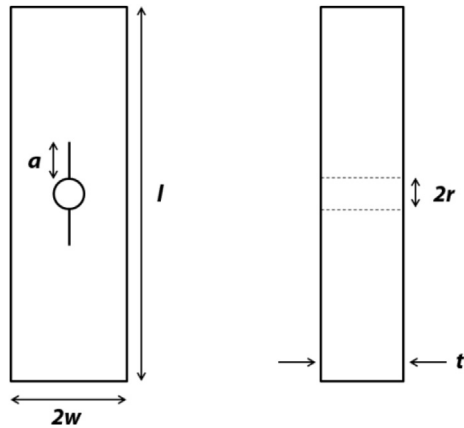**Fig. 2.** DCDC specimen geometry and configuration. a-crack length, l-specimen length, w-specimen half-width, r-hole radius, t-specimen thickness.

specimen until crack arrest occurs near the end of the specimen. The main advantages of the DCDC specimen include mid-plane crack stability and the ability to control the velocity of the advancing crack [34–36,39–42].

Two distinct fracture regimes exist during the DCDC fracture test. There is an initial regime when the crack length is short and the stress necessary for crack growth increases linearly with crack length. Plaisted and co-workers modeled this short crack regime to give the fracture toughness (K_{Ic}) as a function of crack length as [34]:

$$K_{Ic} = \frac{d\sqrt{w}\left(\sqrt{\frac{1+\lambda+e}{1+\lambda-e}} + \sqrt{\frac{1+\lambda-e}{1+\lambda+e}}\right)}{\sqrt{w/r}\sqrt{\pi(1+\lambda)}} \sigma_a(a) \quad (1)$$

where d is a parameter that defines the magnitude of the equivalent force, w is the specimen half-width, r is the hole radius, λ is the normalized crack length (i.e. $\lambda = a/r$), e is a parameter that defines the location of the equivalent force, σ_a is the applied stress and a is the crack length. The parameter d is a function of w/r and is expressed as

$$\frac{d(w/r)}{d_\infty} = 5.7 - 0.75\frac{w}{r} \quad (2)$$

where d_∞ is the value of d in the case of an infinite plate ($d_\infty = 1/\sqrt{27}$) [34].

The second regime in the DCDC test occurs at longer crack lengths where the propagation of the crack tip occurs at nearly constant (plateau) stress. A beam-column analysis was used by Plaisted et al. to create an analytical model for the specimen behavior in this long crack regime. The critical stress intensity factor in this regime is crack length independent and was found to be [34]:

$$K_{Ic} = \frac{2g(w/r)\sqrt{w}}{w/r}\sigma_p \quad (3)$$

where σ_p is the plateau stress obtained from a plot of applied stress versus crack length and $g(w/r)$ is a geometric function given by

$$g(w/r) = \left(\frac{3 + 2\ln(w/r)}{4(w/r)}\right) - \left(\frac{1}{4(w/r)^3}\right). \quad (4)$$

The crack length independence of fracture toughness in the long crack regime, coupled with the fact that the crack faces re-establish contact after the load has been removed, make the DCDC specimen geometry ideal for examining self-healing in brittle polymers. Plaisted and co-workers have employed this specimen geometry to demonstrate thermal healing of a cross-linked polymer [43] and more recently, Hamilton and co-workers have used the DCDC specimen to demonstrate self-healing in a vascularized polymer [10].

2.4. Specimen fabrication

A predetermined mass of dried microcapsules (see Table 1) was placed between two PMMA sheets. These sheets, with dimensions of 65 × 50 × 6.35 mm, were machined from commercial PMMA. The resulting PMMA mold was then sealed with a silicone rubber gasket (3.175 mm thick). The mold was subsequently flushed with argon for approximately 1 min.

Pre-polymerized linear PMMA (Section 2.2) was then injected into the sealed mold containing the microcapsules and the mold was purged again for 45 s. The time between preparing the linear PMMA solution and injecting it into the mold was limited to less than 5 min to prevent the PMMA from polymerizing within the vial. An inversion technique was employed to uniformly distribute the microcapsules throughout the PMMA during the early stages of polymerization in which the mold was inverted 2–3 times at 20 min intervals until the microcapsules no longer sank to the bottom of the mold. At that point, the mold was placed in the refrigerator at 4 °C for at least 12 h to complete the PMMA polymerization. The lower ambient temperature was necessary to dissipate the heat produced during polymerization which can lead to voids in the specimens.

After polymerization, the microcapsule-loaded PMMA specimens were cut to their final DCDC dimensions of 50 × 15.5 × 11 mm with a 4 mm diameter hole drilled through the center (see Fig. 3a) and then polished along the edges to facilitate optical imaging. An image of a DCDC specimen acquired prior to testing is shown in Fig. 3b. The linear PMMA with embedded microcapsules is sandwiched between the two commercial PMMA sheets. Immediately before testing, sharp pre-cracks were introduced at the top and bottom crowns of the central hole by tapping a double-edged razor blade into notches scored at the crowns.

Two types of control specimens were also prepared. The first control was neat PMMA (designated "Neat") that contained no microcapsules. The second type of control specimen (designated "Control") contained 5 wt% microcapsules with a non-healing liquid core of dicyclopentadiene (DCPD) monomer.
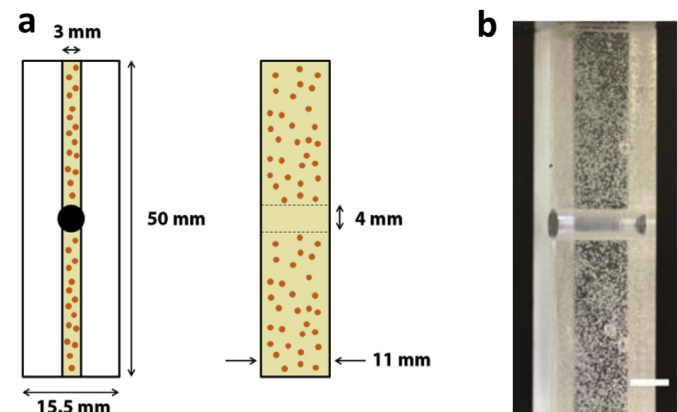

Fig. 3. Self-healing DCDC specimens for fracture testing. (a) Specimen geometry and configuration. (b) Optical image of a linear PMMA specimen containing 5 wt% PMMA-anisole microcapsules. Scale bar: 5 mm.

Table 2
Material properties of PMMA used during tests.

Specimen	Microcapsule core	Microcapsule concentration (wt%)	E' (GPa)	T_g (°C)
Neat	None	–	1.23	95
Self-healing	PMMA-anisole	2.5	1.00	93
	PMMA-anisole	5.0	0.81	92
	PMMA-anisole	7.5	1.07	91
	PMMA-anisole	10.0	0.79	79

2.5. DMA and DCDC testing

Dynamic mechanical analysis (DMA) was used to measure the storage modulus (E') and glass transition temperature (T_g) of the neat and microcapsule-loaded PMMA. Rectangular specimens of dimensions 15 × 3 × 2.3 mm were subjected to 3-point bend testing (10 mm support span) and oscillated at 0.1% maximum strain. The storage modulus for each material type was determined as the value of E' at 1 Hz during a frequency sweep from 0.1 Hz to 90 Hz. The glass transition temperature was obtained from the temperature value at the peak of tan δ ($=E''/E'$) during a temperature sweep from 25 °C to 150 °C at 3 °C/min.

DCDC fracture tests were performed under displacement control using a 150 kN Instron screw-driven load frame (Model 4483). Specimens containing microcapsules were loaded at a constant displacement rate of 20 μm/s while neat specimens were loaded at a constant rate of 15 μm/s. Load and displacement data were collected at 0.5 s intervals. Images of the specimens were acquired at 5 s intervals during testing using a Canon EOS 7D digital camera with a Canon 100 mm Macro lens. These images were used to measure crack length using the image processing software ImageJA (version 1.45b). The first crack length measurement for each specimen was acquired at the first detectable indication of crack propagation. The virgin test was stopped when the load on the specimen stopped increasing. Stress was calculated based on the applied load and the undeformed specimen dimensions. Plots of applied stress (σ) as a function of normalized crack length (a/r) were then generated. The plateau stress for each specimen (σ_p) was obtained from these plots and used to calculate the virgin fracture toughness (K_{Ic}^{Virgin}) using Equation (3). The final crack length of each virgin specimen was also noted.

The effects of healing time and microcapsule concentration on fracture toughness and healing efficiency were investigated. To determine the effect of healing time, virgin specimens containing 5 wt% PMMA-anisole microcapsules were tested and then allowed to heal at room temperature for a time period ranging from 1 to 7 days. During this healing time the specimens were placed on their sides with the crack plane horizontally oriented. At the end of the healing period, specimens were tested again under the same loading conditions as the virgin test, but without introducing a pre-crack prior to testing. The healed test was stopped when the load on the specimen stopped increasing.

The fracture toughness of the healed specimens (K_{Ic}^{Healed}) was evaluated in one of two ways depending on the behavior of the crack propagation through the healed material. For specimens where there was a linear increase in stress with crack growth through the healed material, i.e. over the length of the virgin crack, the short crack model was used to determine K_{Ic}^{Healed} (Equation (1)). For specimens where the crack propagated through the healed material at a relatively constant (plateau) stress, the long crack model was used to determine K_{Ic}^{Healed} (Equation (3)).

The healing efficiency (η) in all cases was calculated as the ratio of the healed fracture toughness to the virgin fracture toughness:

$$\eta = \frac{K_{Ic}^{Healed}}{K_{Ic}^{Virgin}} \tag{5}$$

Specimens with increasing concentrations of microcapsules (from 0 to 10 wt%) were also tested to determine the effect of microcapsule concentration on fracture toughness and healing efficiency. An identical protocol as described above was followed for the virgin and healed tests, but the healing time was fixed at 3 days.

Virgin and healed tests of both types of control specimens (Neat and Control) were also performed with an allowed healing time of 3 days. Reference specimens were also tested in which a solution of PMMA-anisole was manually injected into the crack plane of neat specimens and allowed to heal for 3 days before performing the healed fracture tests.

2.6. Imaging

Scanning Electron Microscope (SEM) images of the fracture surfaces of representative healed specimens were acquired using a Philips XL30 ESEM-FEG field emission environmental Scanning Electron Microscope. SEM images of select specimens were also acquired after virgin testing for crack separation measurements.
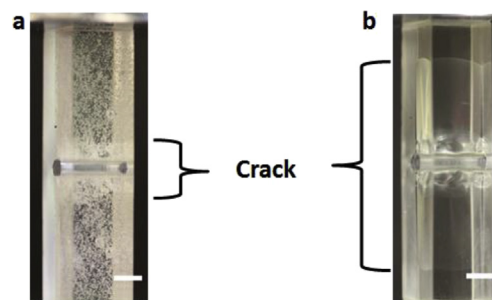
3. Results and discussion

3.1. DMA tests

The effect of the concentration of microcapsules on the material properties of the linear PMMA is illustrated in Table 2. A decrease in storage modulus is observed with increasing microcapsule concentration as expected. The glass transition temperature shows a modest decrease with the largest reduction occurring at 10 wt% microcapsule concentration.

3.2. Virgin tests

Representative images of a self-healing specimen and a neat PMMA specimen acquired after virgin testing are shown in Fig. 4. In

Fig. 4. Linear PMMA DCDC specimen after virgin testing. (a) Self-healing specimen with 5 wt% PMMA-anisole microcapsules. (b) Neat specimen (with no microcapsules). Scale bars 5 mm.
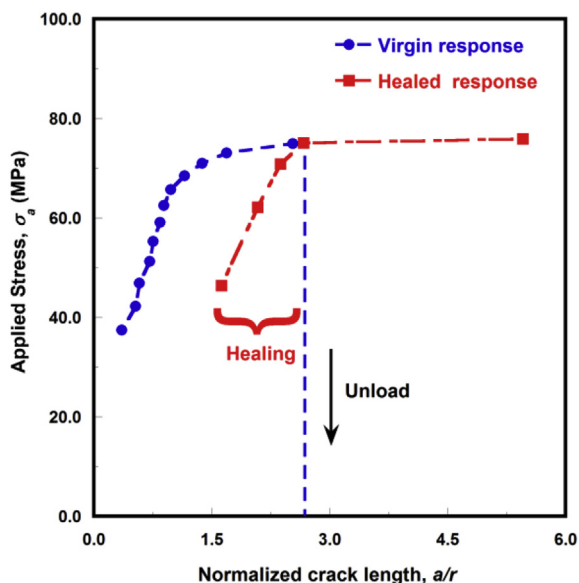
Fig. 5. Representative applied stress versus normalized crack length plot for a self-healing specimen containing 5 wt% PMMA-anisole microcapsules with a heal time of 3 days.
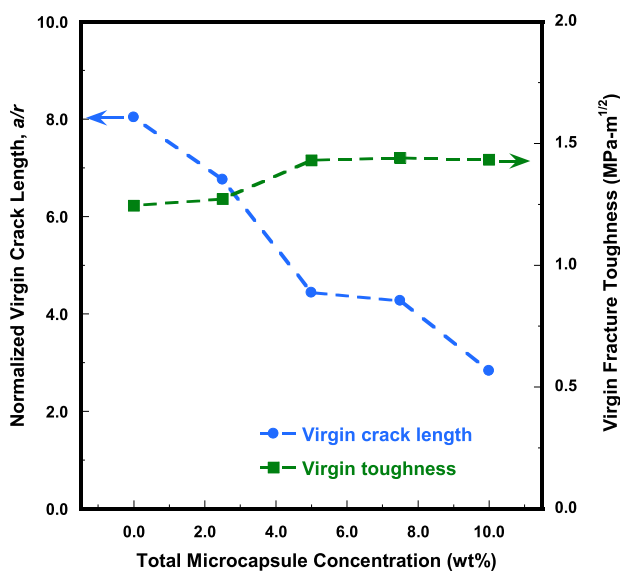

Fig. 6. Effect of microcapsule concentration on final virgin crack length and virgin fracture toughness.
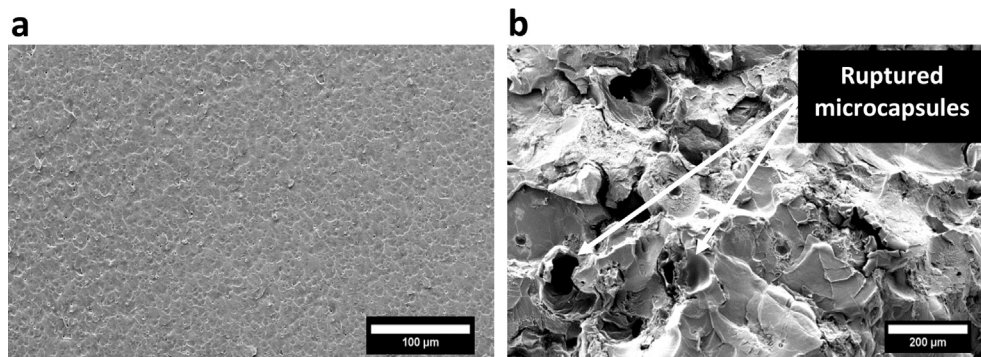
Table 3
Effect of final virgin crack length on healing response for self-healing specimens only.

Normalized virgin crack length (a/r)	# Specimens	% Specimens healed
Less than 2.0	1	100
2.0–4.0	12	66.7
4.0–6.0	6	100
6.0–8.0	2	0
Greater than 8.0	8	0

both, the central crack that has propagated through the midplane of the specimen is clearly visible. The characteristic parabolic shape of the crack front that is usually observed in DCDC specimens of brittle materials [34,44], is apparent in the neat specimen (Fig. 4b), but is absent in the self-healing specimen (Fig. 4a).
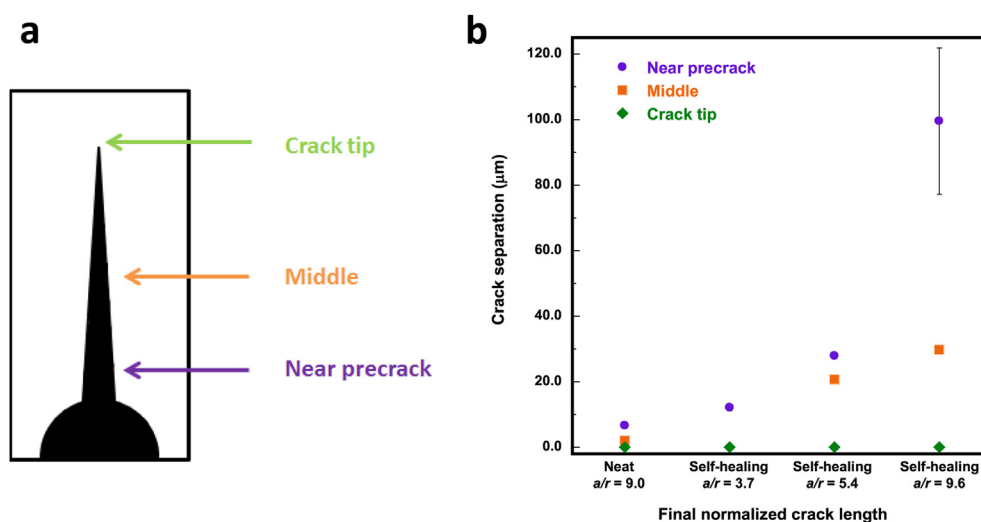
The virgin and healed test results of a self-healing specimen containing 5 wt% PMMA-anisole microcapsules are shown in Fig. 5. During the virgin test there is a linear increase in applied stress with crack length in the short crack regime. With continued loading, the applied stress reaches a plateau value as crack propagation continues (long crack regime). At the end of the virgin testing, the specimen is unloaded and allowed to heal under ambient conditions for 3 days. Upon retesting the healed specimen, the stress increases monotonically until reaching a plateau value with continued crack propagation beyond the healed region.

On average, the final virgin crack lengths of neat PMMA specimens were significantly larger than that of self-healing specimens (see Fig. 6). This result suggests that the microcapsules provided a toughening effect to the matrix, thus reducing the amount of crack growth during testing. A comparison between the virgin fracture toughness of the neat and microcapsule-loaded specimens supports this hypothesis. Specimens containing at least 5 wt% microcapsules are observed to exhibit noticeably higher virgin fracture toughness compared to neat specimens.

The fracture surfaces of neat and self-healing specimens (5 wt% microcapsules) are compared through SEM imaging in Fig. 7. The fracture surface of a neat PMMA specimen is relatively smooth and featureless (see Fig. 7a). In stark contrast, the fracture surface of a self-healing specimen (5 wt% microcapsules) is extremely rough indicating large scale deformation of the matrix material (Fig. 7b). There is also ample evidence of ruptured microcapsules across the fracture surface.

3.3. Self-healing tests

One key finding from the self-healing tests was that the final virgin crack length of the microcapsule-loaded specimens had a

Fig. 7. SEM images of fracture surfaces after healing. (a) Fracture surface of a neat PMMA specimen. (b) Fracture surface of a self-healing specimen containing 5 wt% PMMA-anisole microcapsules.

Fig. 8. Crack separation measurements. (a) Schematic of measurement locations (b) Crack separation as a function of specimen type and normalized crack length. Error bars reflect one standard deviation of data.

significant impact on the healing performance. In Table 3, a summary of the percentage of specimens which displayed some measure of healing is shown as a function of the final virgin crack length. Specimens where the final virgin crack length exceeded a normalized value of 6.0 (i.e. $a/r > 6.0$) showed no healing regardless of the healing time or microcapsule concentration used. A possible reason for this lack of healing in specimens with longer cracks is that the crack separations in these instances were too large and as such, the crack faces could not re-establish contact upon removal of the load [32,45]. As a result, only specimens with normalized virgin crack lengths of 6.0 or lower were used for subsequent data analysis. A summary of crack separation data collected for one neat and three self-healing specimens acquired via SEM imaging is shown in Fig. 8. The crack separation increases considerably for specimens with large final crack lengths.

For the specimens which demonstrated some measure of healing, we observed both short crack and long crack regimes during crack propagation. For example, the self-healing results displayed in Fig. 5 are classified as a short crack response since the stress monotonically increases with crack length up to the end of the healed material region. Thus, the short crack model (Equation (1)) was used to evaluate the healed fracture toughness of this specimen, and others like it, using the maximum crack length and maximum stress value in that region. Alternatively, the self-healing response displayed in Fig. 9 (for a reference specimen) is typical of the long crack model since the stress reaches a plateau as the crack propagates through the healed material. Thus, the long crack model (Equation (3)) was used to determine the healed fracture toughness of this specimen and others like it.
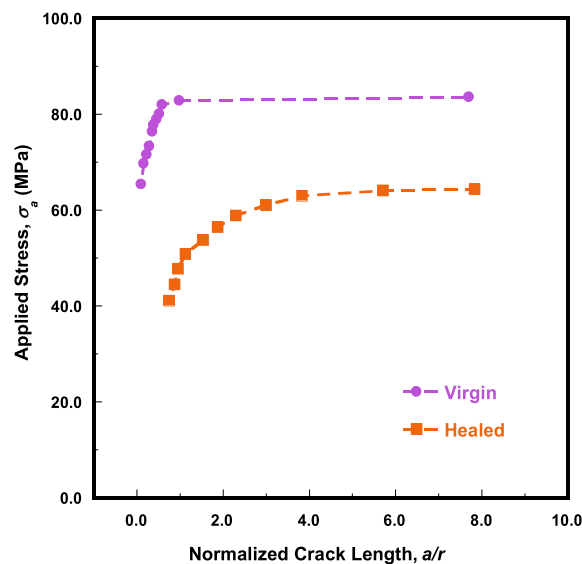
3.4. Effect of healing time

Plots of the virgin and healed fracture toughness, as well as the corresponding healing efficiencies as functions of healing time are shown in Fig. 10. All specimens contained 5 wt% PMMA-anisole microcapsules. The average virgin fracture toughness across all specimens was determined to be 1.41 MPa-m$^{1/2}$. The healed fracture toughness is consistently lower than the virgin toughness for all healing times investigated (see Fig. 10a). An improvement in healed fracture toughness (and healing efficiency) is observed from 1 to 3 days of healing time. This initial improvement in toughness is in agreement with results presented throughout the self-healing
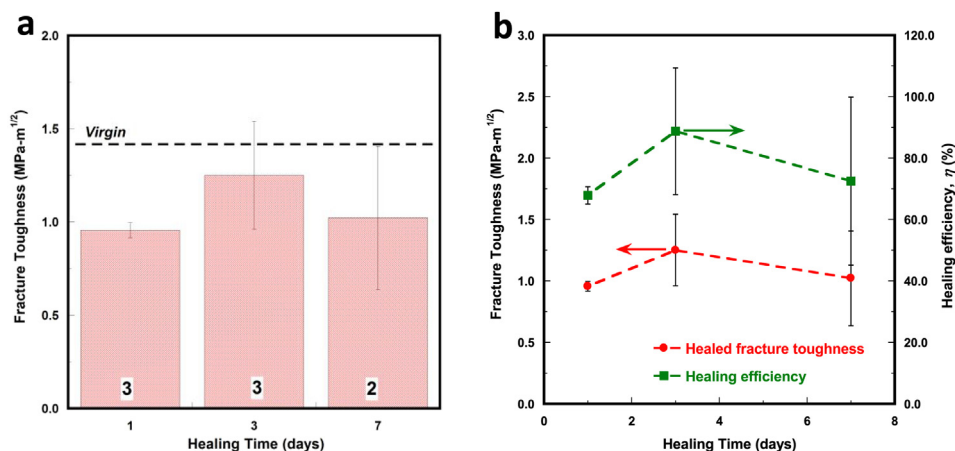
literature where the fracture toughness of the healed material is shown to increase with healing time [25,27,46,47]. The dependence of healing on allowable time has been shown to be largely controlled by diffusion of the interpenetrating chains [27]. The fracture toughness of the specimens allowed to heal for 7 days shows no improvement and is highly scattered due to a limited data set (n = 2).

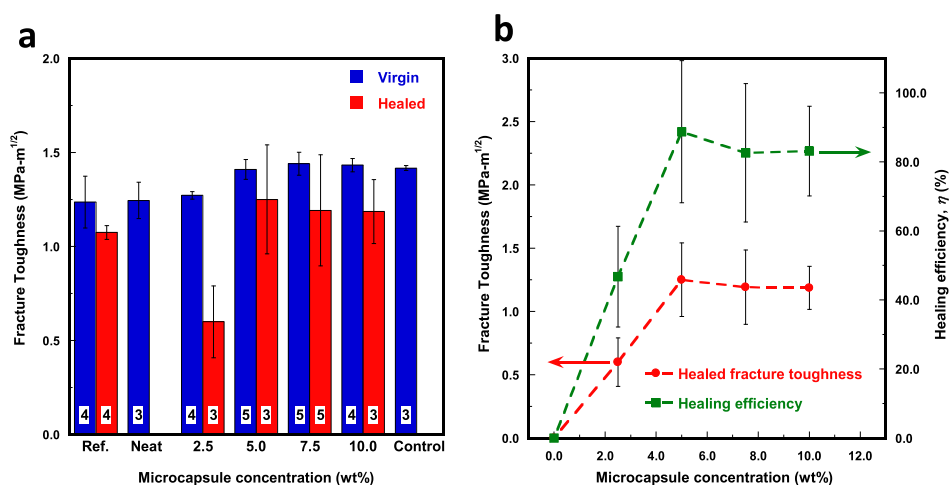### 3.5. Effect of microcapsule concentration

The effect of microcapsule concentration on healing efficiency was investigated by maintaining a consistent healing time of 3 days and varying microcapsule concentrations from 0 to 10 wt%. Fig. 11 shows a summary of the results. Increased virgin toughness is observed for specimens containing at least 5 wt% solvent microcapsules. The virgin fracture toughness increases to approximately 1.43 MPa-m$^{1/2}$ for microcapsule concentrations of 5 wt% and above,

Fig. 9. Representative applied stress versus normalized crack length plot illustrating the long crack response exhibited by a reference specimen in which PMMA-anisole solvent solution was injected into the crack plane after the virgin test.

Fig. 10. Effect of time on healed response of self-healing specimens containing 5 wt% PMMA-anisole microcapsules. (a) Effect of healing time on virgin and healed fracture toughness. The numbers at the bottom of each column denote the number of specimens used in determining the average and standard deviation. (b) Effect of healing time on healing efficiency. Error bars in both plots reflect one standard deviation of data.

Fig. 11. Effect of microcapsule concentration on healed response. (a) Effect of microcapsule concentration on virgin and healed fracture toughness for specimens with a heal time of 3 days. (*Note*: Ref. denotes reference specimens in which the PMMA-anisole healing agent is manually injected into the crack plane). The numbers at the bottom of each column denote the number of specimens used in determining the average and standard deviation. (b) Effect of microcapsule concentration on healing efficiency for self-healing specimens with a heal time of 3 days. Error bars reflect one standard deviation of data.

but does not continue to increase with microcapsule concentration. For all microcapsule concentrations tested, there is significant recovery of toughness after healing, but the healed fracture toughness is consistently lower than the virgin toughness.

A maximum healing efficiency of 89% is achieved for specimens containing 5 wt% microcapsules with 3 days of healing (see Fig. 11b). Increasing the microcapsule concentration beyond 5 wt% provides no further improvement in the healing efficiency. The relatively constant value of η for concentrations of 5 wt% and higher suggests that the volume of solvent released at 5 wt% microcapsule loading is sufficient to mobilize the polymer chains across the fracture plane, heal the damage and recover the virgin properties of the system.

While it was expected that the reference specimens would exhibit near perfect recovery of toughness, this is not reflected in the results (Fig. 11a). The average healing efficiency for the reference specimens is calculated to be 88%. Two possible causes of this reduction in performance are insufficient filling of the entire crack plane during the injection of the PMMA-anisole solvent solution and imperfect registration of the crack surfaces after fracture. In

both cases, the polymer chains would not be adequately swollen and mobilized across the crack plane to recover the virgin properties of the material. As expected, the control specimens show no recovery of fracture toughness after healing.

4. Conclusions

The efficacy of solvent-based self-healing in linear PMMA was investigated. Microcapsules containing a PMMA-anisole liquid core were incorporated into linear PMMA and the fracture toughness of virgin and healed specimens was evaluated using the double cleavage drilled compression (DCDC) test protocol. The inclusion of microcapsules improved the toughness of the linear PMMA. A short healing time of 3 days produced the best healing results for this solvent healing system. Maximum healing efficiency of 89% was achieved by incorporating 5 wt% PMMA-anisole microcapsules into the PMMA matrix. This substantial recovery of virgin fracture toughness demonstrates the potency of the PMMA-anisole solvent system for healing crack damage in thermoplastic PMMA and

provides a model system for self-healing of other commodity thermoplastic polymers.

References

[1] White SR, Sottos NR, Geubelle PH, Moore JS, Kessler MR, Sriram SR, et al. Autonomic healing of polymer composites. Nature 2001;409(6822):794—7.
[2] Keller MW, White SR, Sottos NR. A self-healing poly(dimethyl siloxane) elastomer. Adv Funct Mater 2007;17(14):2399—404.
[3] Rule JD, Brown EN, Sottos NR, White SR, Moore JS. Wax-protected catalyst microspheres for efficient self-healing materials. Adv Mater 2005;17(2):205—8.
[4] Brown EN, Sottos NR, White SR. Fracture testing of a self-healing polymer composite. Exp Mech 2002;42(4):372—9.
[5] Yuan YC, Rong MZ, Zhang MQ, Chen J, Yang GC, Li XM. Self-healing polymeric materials using epoxy/mercaptan as the healant. Macromolecules 2008;41(14):5197—202.
[6] Caruso MM, Blaiszik BJ, Jin HH, Schelkopf SR, Stradley DS, Sottos NR, et al. Robust, double-walled microcapsules for self-healing polymeric materials. ACS Appl Mater Interfaces 2010;2(4):1195—9.
[7] Toohey KS, Sottos NR, Lewis JA, Moore JS, White SR. Self-healing materials with microvascular networks. Nat Mater 2007;6(8):581—5.
[8] Toohey KS, Hansen CJ, Lewis JA, White SR, Sottos NR. Delivery of two-part self-healing chemistry via microvascular networks. Adv Funct Mater 2009;19(9):1399—405.
[9] Hansen CJ, Wu W, Toohey KS, Sottos NR, White SR, Lewis JA. Self-healing materials with interpenetrating microvascular networks. Adv Mater 2009;21(41):1—5.
[10] Hamilton AR, Sottos NR, White SR. Self-healing of internal damage in synthetic vascular materials. Adv Mater 2010;22(45):5159—63.
[11] Patrick JF, Sottos NR, White SR. Microvascular based self-healing polymeric foam. Polymer 2012;53(19):4231—40.
[12] Pang JWC, Bond IP. A hollow fibre reinforced polymer composite encompassing self-healing and enhanced damage visibility. Compos Sci Technol 2005;65(11—12):1791—9.
[13] Bond IP, Trask RS, Williams HR. Self-healing fiber-reinforced polymer composites. MRS Bull 2008;33(8):770—4.
[14] Jin H, Miller GM, Sottos NR, White SR. Fracture and fatigue response of a self-healing epoxy adhesive. Polymer 2011;52(7):1628—34.
[15] White SR, Moore JS, Sottos NR, Krull BP, Santa Cruz WA, Gergely RCR. Restoration of large damage volumes in polymers. Science 2014;344(6184):620—3.
[16] Jin HH, Mangun CL, Stradley DS, Moore JS, Sottos NR, White SR. Self-healing thermoset using encapsulated epoxy-amine healing chemistry. Polymer 2012;53(2):581—7.
[17] Blaiszik BJ, Kramer SLB, Olugebefola SC, Moore JS, Sottos NR, White SR. Self-healing polymers and composites. Annu Rev Mater Res 2010;40:179—211.
[18] Wilson GO, Caruso MM, Reimer NT, White SR, Sottos NR, Moore JS. Evaluation of ruthenium catalysts for ring-opening metathesis polymerization-based self-healing applications. Chem Mater 2008;20(10):3288—97.
[19] Beiermann BA, Keller MW, Sottos NR. Self-healing flexible laminates for resealing of puncture damage. Smart Mater Struct 2009;18(8):085001.
[20] Cho SH, White SR, Braun PV. Self-healing polymer coatings. Adv Mater 2009;21(6):645.
[21] Cho SH, Andersson HM, White SR, Sottos NR, Braun PV. Polydimethylsiloxane-based self-healing materials. Adv Mater 2006;18(8):997.
[22] Caruso MM, Delafuente DA, Ho V, Sottos NR, Moore JS, White SR. Solvent-promoted self-healing epoxy materials. Macromolecules 2007;40(25):8830—2.
[23] Caruso MM, Blaiszik BJ, White SR, Sottos NR, Moore JS. Full recovery of fracture toughness using a nontoxic solvent-based self-healing system. Adv Funct Mater 2008;18(13):1898—904.
[24] Kumar A, Stephenson LD, Murray JN. Self-healing coatings for steel. Prog Org Coat 2006;55(3):244—53.
[25] Wool RP, O'Connor KM. Time dependence of crack healing. J Polym Sci Polym Lett Ed 1982;20(1):7—16.
[26] Shen JS, Harmon JP, Lee S. Thermally-induced crack healing in poly(methyl methacrylate). J Mater Res 2002;17(6):1335—40.
[27] Wool RP, O'Connor KM. A theory crack healing in polymers. J Appl Phys 1981;52(10):5953—63.
[28] Hsieh HC, Yang TJ, Lee S. Crack healing in poly(methyl methacrylate) induced by co-solvent of methanol and ethanol. Polymer 2001;42(3):1227—41.
[29] Wang PP, Lee S, Harmon JP. Ethanol-induced crack healing in poly(methyl methacrylate). J Polym Sci Part B Polym Phys 1994;32(7):1217—27.
[30] Lin CB, Lee SB, Liu KS. Methanol-induced crack healing in poly(methyl methacrylate). Polym Eng Sci 1990;30(21):1399—406.
[31] Mookhoek SD, Mayo SC, Hughes AE, Furman SA, Fischer HR, van der Zwaag S. Applying SEM-based x-ray microtomography to observe self-healing in solvent encapsulated thermoplastic materials. Adv Eng Mater 2010;12(3):228—34.
[32] Caruso MM. Solvent-based self-healing polymeric materials [Ph.D. Thesis]. U.S.A: University of Illinois at Urbana-Champaign; 2010.
[33] Gladman AS, Celestine AN, Sottos NR, White SR. Autonomic healing of acrylic bone cement. Adv Healthc Mater 2015;4(2):202—7.
[34] Plaisted TA, Amirkhizi AV, Nemat-Nasser S. Compression-induced axial crack propagation in DCDC polymer samples: experiments and modeling. Int J Fract 2006;141(3—4):447—57.
[35] Pallares G, Ponson L, Grimaldi A, George M, Prevot G, Ciccotti M. Crack opening profile in DCDC specimen. Int J Fract 2009;156(1):11—20.
[36] Ayatollahi MR, Bagherifard S. Numerical analysis of an improved DCDC specimen for investigating mixed mode fracture in ceramic materials. Comput Mater Sci 2009;46(1):180—5.
[37] Crichton SN, Tomozawa M, Hayden JS, Suratwala TI, Campbell JH. Subcritical crack growth in a phosphate laser glass. J Am Ceram Soc 1999;82(11):3097—104.
[38] Warren WE. Theoretical-analysis of the double cleavage drilled compression specimen. Int J Fract 1987;33(3):223—35.
[39] He MY, Turner MR, Evans AG. Analysis of the double cleavage drilled compression specimen for interface fracture energy measurements over a range of mode mixities. Acta Metall Mater 1995;43(9):3453—8.
[40] Marliere C, Despetis F, Phalippou J. Crack path instabilities in DCDC experiments in the low speed regime. J Non Cryst Solids 2003;316(1):21—7.
[41] Nielsen C, Amirkhizi AV, Nemat-Nasser S. The effect of geometry on fracture strength measurement using DCDC samples. Eng Fract Mech 2012;91:1—13.
[42] Jenne TA, Keat WD, Larson MC. Limits of crack growth stability in the double cleavage drilled compression specimen. Eng Fract Mech 2003;70(13):1697—719.
[43] Plaisted TA, Nemat-Nasser S. Quantitative evaluation of fracture, healing and re-healing of a reversibly cross-linked polymer. Acta Mater 2007;55(17):5684—96.
[44] Tian Q, Rong MZ, Zhang MQ, Yuan YC. Synthesis and characterization of epoxy with improved thermal remendability based on Diels-Alder reaction. Polym Int 2010;59(10):1339—45.
[45] Hamilton AR. Mechanical characterization and self-healing in synthetic vascularized materials. U.S.A: University of Illinois at Urbana-Champaign; 2011.
[46] Jud K, Kausch HH. Load transfer through chain molecules after interpenetration at interfaces. Polym Bull 1979;1(10):697—707.
[47] Jud K, Kausch HH, Williams JG. Fracture mechanics studies of crack healing and welding of polymers. J Mater Sci 1981;16(1):204—10.